# Passivated, Highly Reflecting, Laser Contacted Ge Rear Side for III-V Multi-Junction Solar Cells

Charlotte Weiss, Jonas Schön, Oliver Höhn, Bianca Fuhrmann, Frank Dimroth, and Stefan Janz

***Abstract*—This article describes the successful integration of a passivated, highly reflecting Ge rear side into a III-V multijunction solar cell. The use of lowly doped Ge and the new rear side leads to the aimed increase in Ge cell current up to 1.6 mA.cm$^{-2}$, demonstrated by external quantum efficiency and *I–V* measurements. For the contact formation, two different types of laser processes were conducted and evaluated—the laser fired contact route and the PassDop route. In both cases, the formation of a local back surface field preserves the passivation of the contact points. A laser pitch and laser power variation leads to a good performing back contact. The passivation effect is proven experimentally and is qualitatively accessed with cell simulations.**

***Index Terms*—III-V multijunction solar cells, germanium, laser contacts, surface passivation.**

## I. Introduction

TO ACCOMPLISH the continuous improvement of III-V solar cells, the focus is mainly on the development of the III-V layer stack, for example by adding more junctions [1]–[3]. However, the focus of this article is the improvement of the rear side of Ge-based III-V solar cells. The aimed improvement is the increase of Ge cell current. The rear side processes to achieve this aim include thin film deposition, metallization, and laser contact formation. These processes are well known in Si terrestrial photovoltaics and promise therefore a reliable and cost-efficient integration into the Ge-based III-V cell process chain. The rear side treatment starts with the deposition of a Si-based passivation layer to reduce the recombination of minority carriers at the Ge rear side, followed by the deposition of a mirror layer stack, consisting of another Si-based layer and an Al layer which acts as both, mirror layer and electrical contact.

A successful decrease in recombination due to the passivation layer will lead to an increase in current of the Ge cell. This additional current from the Ge cell will not increase the cell efficiency of state-of-the-art three junction space solar cells [4], as they are not current limited by the Ge cell. However, going to metamorphic three junction cells [5] or to four or more junctions, the increased Ge current will directly influence the overall cell performance [6].

An inevitable precondition for increasing the Ge cell current is the use of lowly doped Ge wafers. In normal Ge-based solar cells, the Ge wafer has a typical doping level of $2 \times 10^{17}$at.cm$^{-3}$ and a thickness of 140 $\mu$m. In these wafers, a significant part of the incoming photons is absorbed by free carrier absorption (FCA) and cannot contribute to the formation of charge carriers. Therefore, for our rear side concept, the Ge doping level was reduced to $2 \times 10^{16}$ at.cm$^{-3}$. The lower doping concentration results in smaller FCA [7] (and references therein).

The Al mirror at the Ge rear side ensures a high reflectivity of photons. The reflected photons will pass through the Ge cell a second time and those with energies higher than the bandgap of Ge ($E_G = 0.67$ eV) will have a second chance to be absorbed. Reflected photons with energies lower than $E_G$ will be out-reflected instead of being absorbed in the Ge bulk or at the metal contact. As a consequence, the cell temperature under operation is reduced and the voltage increased. It was shown recently that a rear side mirror similar to the one in this article leads to a temperature decrease in a space solar cell in operation of about 9 K [8].

The development and the performance of the passivation layer and the simulated cell potential were described earlier [9]–[11]. Furthermore, the improved rear side was recently integrated successfully into a four junction solar cell device [6]. In this article, we focus on the general integration of the additional rear side processes in the III-V cell process chain, on the optimization of these processes and on a detailed discussion of the improved Ge cell performance. To keep the cell results as universal as possible, we conduct the whole study using Ge-isotypes. This allows for an easy and reliable access to the Ge bottom junction performance with current/voltage (*I–V*), external quantum efficiency (EQE) and reflection measurements. For contacting the passivated isotypes, we use two routes, the laser fired contacts (LFCs) and the PassDop contacts. The main difference between LFC and PassDop contacts is the moment of the laser process. For LFC, both the dielectric passivation layer and the Al contact are deposited and then the laser process takes place. For PassDop contacts, already the dielectric passivation is opened with the laser process and the Al layer is deposited afterwards. For further information about LFC [12] and PassDop contacts [13], [14], the reader is referred to Si literature. In both cases, the laser process leads to a highly p-type ($p^+$) doped region under each contact point, realized by Al atoms for LFC contacts and by Boron atoms for PassDop contacts. These $p^+$-doped regions compensate for the locally destroyed passivation layer under the metal contact

Manuscript received November 19, 2020; revised March 7, 2021 and April 9, 2021; accepted April 21, 2021. Date of publication July 12, 2021; date of current version August 20, 2021. This work was supported by the European Union's Horizon 2020 research and innovation program within the project SiLaSpaCe under Grant Agreement 687336. *(Corresponding author: Charlotte Weiss.)*

Charlotte Weiss, Jonas Schön, Oliver Höhn, and Frank Dimroth are with the Fraunhofer Institute for Solar Energy Systems, 79110 Freiburg, Germany (e-mail: charlotte.weiss@ise.fraunhofer.de; jonas.schoen@ise.fraunhofer.de; oliver.hohen@ise.fraunhofer.de; frank.dimroth@ise.fraunhofer.de).

Bianca Fuhrmann is with Azur Space Solar Power GmbH, 74072 Heilbronn, Germany (e-mail: bianca.fuhrmann@azurspace.com).

Color versions of one or more figures in this article are available at https://doi.org/10.1109/JPHOTOV.2021.3087727.

Digital Object Identifier 10.1109/JPHOTOV.2021.3087727

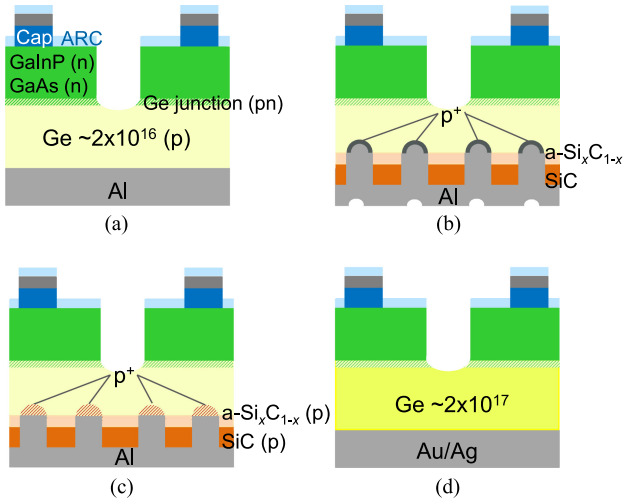


Fig. 1. Structure of the Ge-isotypes used in this work. (a) AlOnly cells, (b) cells with LFC contact. (c) Cells with PassDop contact. (d) Standard cells.

points, creating a local back surface field (LBSF) and therefore a field effect passivation. This mechanism is expected to occur in case of Ge analogously to Si, as Al and B atoms are p-type dopants in Ge [15], [16]. Optoelectrical simulations are used to analyze the passivation and mirror quality of the samples.

The Ge-isotypes with the improved rear side can later be integrated into any cell concept which profits from the new rear side without any further process adaption.

## II. Methods

### A. Sample Description

On test samples we showed good passivated Ge surfaces leading to effective minority carrier lifetimes of $\tau_{\text{eff}} > 300\ \mu$s on Ge with a doping level of $2 \times 10^{16}$ at.cm$^{-3}$ [9]–[11] as well as ohmic, low resistance contacts. For this article, the developed rear side structure was implemented into a III-V multijunction (MJ) solar cell process. For easy access to the performance of the Ge subcell, so-called Ge-isotypes were produced. These are Ge subcells with III-V epitaxy on top which filters the spectrum to show a comparable Ge response as in a 3G30 MJ cell from AZUR [4].

For this article, three batches of isotypes were prepared: nonpassivated isotypes with a full-area Al rear side of ≈1 µm thickness, called "AlOnly" in the following [see Fig. 1(a)]; LFC isotypes [see Fig. 1(b)] and PassDop isotypes [see Fig. 1(c)]. For all three isotypes, the resistivity of the Ge substrates is ≈0.2 Ωcm ($2 \times 10^{16}$ at.cm$^{-3}$) and the wafers are delivered by the manufacturer Umicore. For comparison, the isotype of an AZUR standard 3G30 cell with a Ge resistivity of ≈0.03 Ωcm ($2 \times 10^{17}$ at.cm$^{-3}$) and an evaporated Au/Ag back contact [see Fig. 1(d)] is used. All cells investigated in this article have a size of $2 \times 2$ cm². For all isotypes, the epitaxial layer stack [GaAs/GaInP (both n-doped)] is grown by a metalorganic vapour-phase epitaxy (MOVPE) process on the front side of the Ge wafer. At the Ge/GaAs interface, a pn-junction comparable to the one described by Friedman and Olson [17] is formed. The rear side treatment is different for the different batches of

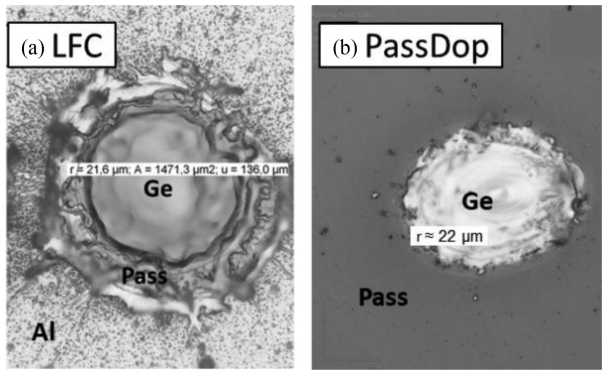


Fig. 2. Microscopy images of (a) a well performing LFC contact and (b) a well performing PassDop contact.

isotypes: On the rear side of the LFC and PassDop wafers, an a-$Si_{0.97}C_{0.03}$:H (30 nm) passivation layer and an a-$Si_{0.50}C_{0.50}$:H (125 nm) mirror layer stack is provided by plasma enhanced chemical vapour deposition with a subsequent furnace annealing step at 400 °C. The AlOnly and standard isotypes do not have a dielectric layer on the rear side. Then, the front side processing is conducted for all isotypes, which consists of cap etching, metallization and the deposition of antireflection coating of $TiO_x/Al_2O_3$. With mesa etching, the wafer is divided into $12\times$ ($2 \times 2$) cm² cells. For rear side processing of LFC cells [see Fig. 1b)], an Al layer with a thickness ≈1 $\mu$m is deposited by thermal evaporation. The following laser process drives the Al through the passivation and the mirror layer into the Ge substrate. A contact point with a LBSF is formed, because the dissolved Al forms a $p^+$-doped Ge region beneath the metal contact points. For rear side processing of PassDop cells [see Fig. 1(c)], the laser induced contact formation is conducted directly after the deposition of passivation and mirror layers. As the layer stack is boron doped, the formation of a LBSF with the help of the dopant boron is expected. A full area Al back contact with a thickness ≈1 $\mu$m is deposited as a last process step of the PassDop concept.

The laser power of 2.1/0.9 W, pulse frequency of 10/8 kHz and pulse duration of 120/600 ns was chosen for LFC/PassDop, because it is the minimum power that leads to a successful opening of the passivation layer and radial shaped laser contacts with a radius of around 22 $\mu$m [see Fig. 2(a) and (b)]. Contacts formed under these conditions are known for good performance from Si technology. In order to find the best laser parameters for the new rear side, the laser contact distance (pitch) is varied for LFC and PassDop isotypes between 500 and 1000 $\mu$m. This leads to an area covered with contacts between 0.6 and 0.2% of the passivated back side. For the laser power variation experiment on LFC isotypes, the laser frequency and pulse duration are the same as for the pitch variation and two pitches (900 and 1000 $\mu$m) were used. The laser power was increased from 2.1 to 7.0 W, leading to an increase of the contact radius up to 35 $\mu$m. This corresponds to an area covered with contacts of 0.5/0.4% for a pitch of 900/1000 $\mu$m.

In the case of AlOnly cells [see Fig. 1(a)] and standard cells [see Fig. 1(d)], a full area Al contact and an Ag/Au contact is deposited directly on the Ge rear side, respectively. For the measurements, all cells are separated by chip sawing. As the standard cells were not produced for this article, only the AlOnly,

TABLE I
PARAMETERS USED FOR THE SOLAR CELL SIMULATIONS

| | Standard | AlOnly | LFC | PassDop |
|---|---|---|---|---|
| Base doping | $2x10^{17}$ $cm^{-3}$ | $2x10^{16}$ $cm^{-3}$ | $2x10^{16}$ $cm^{-3}$ | $2x10^{16}$ $cm^{-3}$ |
| e- lifetime (base) | 4 µs [9] | 340 µs [10] | 340 µs [10] | 340 µs [10] |
| e- mobility | 2433 $cm^2/s$ [19] | 3232 $cm^2/s$ [19] | 3232 $cm^2/s$ [19] | 3232 $cm^2/s$ [19] |
| Surface recombination velocity | $10^7$ cm/s ($\approx v_{thermal}$) | $10^7$ cm/s ($\approx v_{thermal}$) | 900 cm/s (fit) | 900 cm/s (fit) |
| External $R_S$ | 0.6 $\Omega cm^2$ (std) | 0.6 $\Omega cm^2$ (std) | 0.9 $\Omega cm^2$ (fit) | 0.6 $\Omega cm^2$ (std) |

LFC and PassDop isotypes have exactly the same epitaxial layers and the same front side process steps. It is important to keep that in mind when the three groups of lowly doped isotypes are compared to the standard cells in the following results and discussion section.

### B. Solar Cell Simulations

For the in-depth analysis of the implemented mirror and surface passivation at the Ge rear side, a 2-D optoelectrical model for a Ge solar cell was implemented in Sentaurus Device [9], [18]. The two cells above the Ge cell are optically modeled, whereas the Ge cell itself is modeled optically and electrically using measured Ge bulk lifetimes [9], [10]. The input parameters for the cell simulation are given in Table I. The contact resistance at the front and rear side as well as the finger resistance is not explicitly simulated. Instead these effects are combined in an external series resistance $R_S$ which has typical value of 0.6 $\Omega cm^2$, if not stated otherwise.

The optical transfer-matrix method is extended assuming rough Ge interfaces that cause incoherent light scattering [18]. In case of the aluminum rear side the Al layer is explicitly modeled in the optical simulations. In our 2-D simulations we neglect the worse reflectivity at the rear point contacts and the lateral transport losses in the base by assuming a full contact. Thus, our simulation corresponds to an infinitely small contact distance (pitch). In the electrical simulations we use the measured $e^-$ lifetime for Ge from [9] and [10]. For the standard Ge cell, we assume no surface passivation at the rear side, i.e., a recombination velocity of $10^7$ cm/s. The surface recombination velocity (SRV) in case of a SiC passivation layer is determined to match the improvements in $V_{OC}$. Hence, the simulation gives access to the passivation quality of the Ge rear side in the cell, which is not accessible experimentally.

### C. Measurement Parameters of Ge-Isotype Cells

The *I–V* characteristics in this article were measured with a four sources sun simulator under AM0 spectral conditions at 28 °C. From the *I–V* curves, the following cell parameters were extracted: Short-circuit current ($I_{SC}$); open circuit voltage ($V_{OC}$); fill factor (FF); and efficiency ($\eta$).

The EQE was measured under colored bias light and under bias voltage. The EQE results are calibrated with the $I_{SC}$ from the *I–V* measurements. The reflectance was measured with a Lambda900 spectrometer of the manufacturer PerkinElmer.

## III. RESULTS

### A. I–V Measurements of LFC Isotypes

In Fig. 3, *I-V* characteristic results for an LFC pitch variation from 500 to 1000 $\mu$m at a laser power of 2.1 W are shown. Two pitches were used on one wafer, which leads to six identical cells per pitch.

The results originate from three wafers (violet diamonds, circles and squares) with two pitches, respectively, and one wafer with AlOnly cells (blue pentagons). For comparison, values for a standard 3G30 isotype are plotted (black stars). The results show that short circuit current [see $I_{SC}$, Fig. 3(a)], open-circuit voltage see[$V_{OC}$, Fig. 3(b)], fill factor [see FF, Fig. 3(c)] and efficiency [see $\eta$, Fig. 3(d)] are higher for all pitches used in this experiment, compared to the AlOnly cells with full area contact. $I_{SC}$ increases from about 28 to 29 $mA.cm^{-2}$ (corresponds to $\Delta I_{SC} \approx 1$ $mA.cm^{-2}$) and $V_{OC}$ from 0.19 to 0.25 V (corresponds to $\Delta V_{OC} \approx 60$mV). The measured FF [see Fig. 2(c)] increases from 58% in the AlOnly cell to 60% in the LFC cell.

As a consequence, $\eta$ [see Fig. 3(d)] increases significantly from 2.3 to 3.2%. The dependency of the *I–V* parameter on the pitch is the following: There is a slight decrease of $I_{SC}$ and FF with increasing pitch and a slight increase in $V_{OC}$ with increasing pitch. The $V_{OC}$, $I_{SC}$, and FF effect cancel almost out in the efficiency and lead to a nearly constant $\eta$ for the full pitch range under investigation (500–1000 $\mu$m). The comparison between LFC cell parameter and the standard isotype (black stars) as well as the cell simulations (green line) will be addressed in the discussion section together with the PassDop results.

For LFC samples, also a power variation between 2.1 and 7.0 W is performed with a pitch of 900 and 1000 $\mu$m (results in the appendix). This experiment shows that the smallest power of 2.1 W with smaller pitches lead to better cell performance than higher powers with larger pitches. The results will be included into the discussion about the optimum laser pitch.

### B. I–V Measurements of PassDop Isotypes

In Fig. 4, *I-V* characteristic results for a pitch variation from 500 to 1000 $\mu$m at a laser power of 0.9 W are shown. Two pitches were used on one wafer, which leads to six identical cells per pitch.

The results originate from two wafers (red diamonds and circles) with two pitches, respectively, and one wafer with AlOnly cells, which are the same as in Fig. 3 (blue pentagons). Again, typical values for a standard 3G30 isotype are plotted (black stars). The results show that short circuit current [see $I_{SC}$, Fig. 4(a)], open-circuit voltage [see $V_{OC}$, Fig. 4(b)], fill factor [see FF, Fig. 4(c)], and efficiency [see $\eta$, Fig. 4(d)] are in the same range as for the LFC isotypes and higher than the AlOnly cells for all pitches. $I_{SC}$ increases from about 28 to 29 $mA.cm^{-2}$ (corresponds to $\Delta I_{SC} \approx 1$ $mA.cm^{-2}$) and $V_{OC}$ from 0.19 to 0.24 V (corresponds to $\Delta V_{OC} \approx 50$ mV). The measured FF [see Fig. 4(c)] increases from 58 in the AlOnly cell to 61%

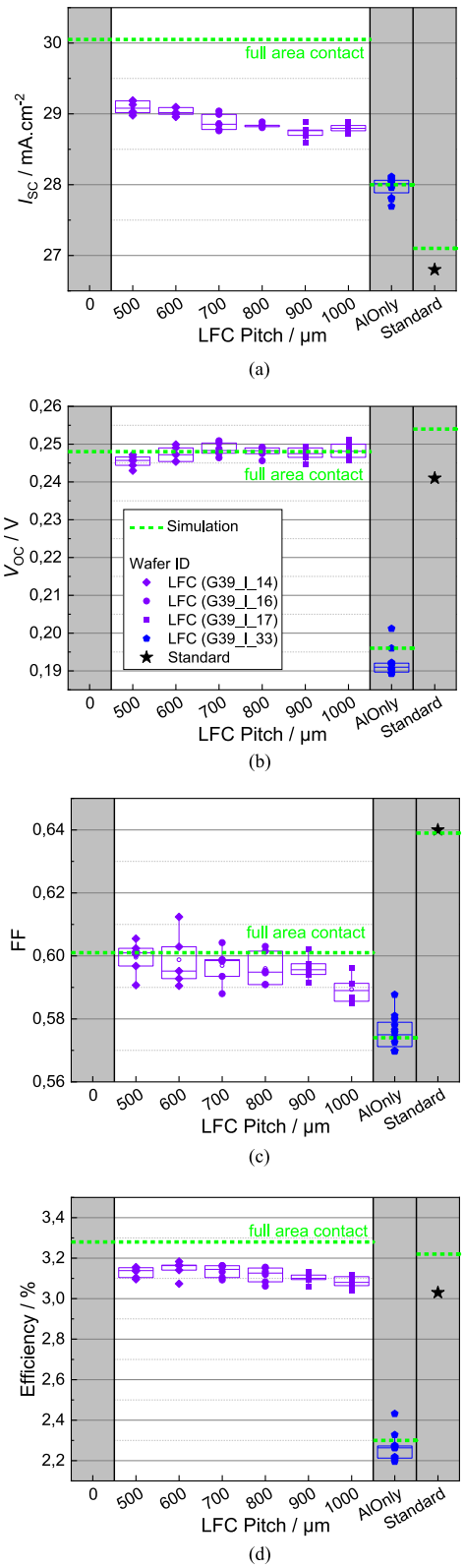


Fig. 3. *I–V* characteristics for Ge-isotypes with LFC rear side and with pitch variation. Violet data points with three different shapes belong to three different wafers. On every wafer, there are 12 cells with two different pitches. Additionally, 12 AlOnly cells (blue pentagons) are measured and typical values for a standard cell (black stars) are depicted. (a) Parameter $I_{SC}$. (b) $V_{OC}$. (c) Fill factor. (d) Efficiency $\eta$. The green line represents the simulation values for a full area contact, which corresponds to a pitch of 0 $\mu$m. Note that a higher external series resistance is used compared to the PassDop solar cell model (see Table I).

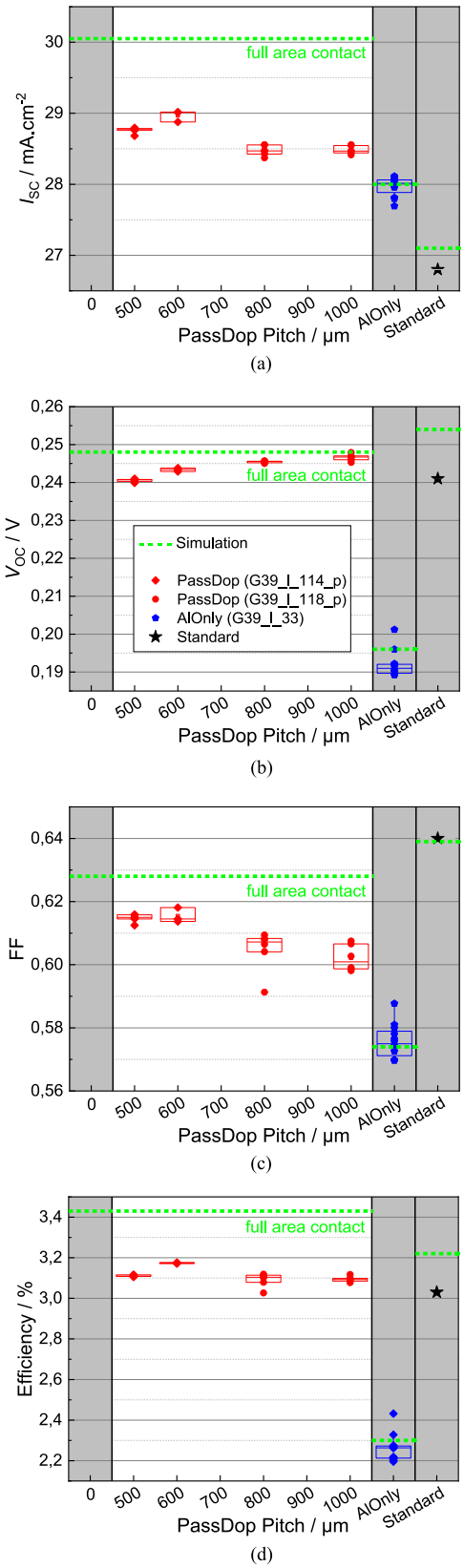


Fig. 4. *I–V* characteristics for Ge-isotypes with PassDop rear side and with pitch variation (red data points). On every wafer, there are 12 cells with two different pitches. Additionally, 12 AlOnly cells (blue pentagons) are measured and typical values for a standard cell (black stars) are depicted. (a) Parameter $I_{SC}$. (b) $V_{OC}$. (c) Fill factor (d) Efficiency $\eta$. The green line represents the simulation values for a full area contact, which corresponds to a pitch of 0 $\mu$m.

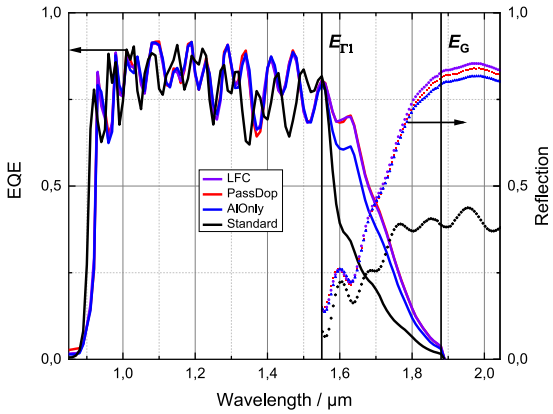


Fig. 5. EQE and %R of a Ge-isotype with passivation and mirror on rear side and a 600 $\mu$m pitch LFC contact (violet), a PassDop contact (red) and a Ge-isotype AlOnly cell without passivation and mirror on the Ge rear side (blue). For comparison, a standard highly doped Ge-isotype cell from AZUR without passivation and with standard rear side metal is depicted (black). The direct ($E_{\Gamma 1}$) and indirect ($E_G$) Ge bandgaps are represented by vertical lines.

in the PassDop cell and $\eta$ [see Fig. 4(d)] increases significantly from 2.3 to 3.1%. $I_{\mathrm{SC}}$, FF and $\eta$ are significantly lower for 800 and 1000 $\mu$m than for 500 and 600 $\mu$m, whereas $V_{\mathrm{OC}}$ shows the opposite trend. For the PassDop samples, the 600 $\mu$m turns out to be the optimum pitch. The comparison between PassDop cell parameter and the standard isotype (black stars) as well as the cell simulations (green line) will be addressed in the discussion section together with the LFC results.

For PassDop samples, no laser power variation was made, due to the results of the LFC laser power variation. This will be explained shortly in the discussion about the optimum laser pitch.

### C. EQE and %R Measurement of Isotypes

EQE and reflectivity measurements were conducted for selected cells from Figs. 3 and 4 and presented in Fig. 5.

For the sake of clarity, we compare only the three cells with the best efficiency from the group of LFC (violet) PassDop (red) and AlOnly cells (blue) with a standard 3G30 cell from AZUR (black). All Ge EQEs show a strong modulation, which is due to thin film interferences in the GaAs/GaInP layers. The fact that the EQEs of the LFC, the PassDop and the AlOnly cell overlay up to wavelengths of 1.55 $\mu$m, indicates that the epi layer stacks are very similar in thickness and therefore a comparison between these cells is reasonable. As expected, the EQE from the AZUR standard cell shows slightly different height and modulations, as this cell was grown in another epitaxy run. For photon energies lower than the direct bandgap ($E_{\Gamma 1} = 0.80$ eV $\triangleq$ 1.55 $\mu$m, vertical line in Fig. 5) of Ge, the intrinsic absorption coefficient of Ge [7], and therefore, the EQE drops significantly. In this wavelength range, the EQEs of the passivated Ge-isotypes (violet and red) overlap and lie significantly above the EQE of the not passivated Ge-isotype (blue). The EQE of the standard cell (black) drops under the EQEs of all three lowly doped isotypes for wavelengths $>$1.55 $\mu$m.

In addition to EQE measurements (straight lines), the reflection of the four Ge-isotypes was measured and depicted in Fig. 5 (dotted lines) in the same colors as the EQE spectra. For this article, the reflection for wavelengths longer than 1.55 $\mu$m (direct bandgap $E_{\Gamma 1}$) is interesting, because photons in this wavelength range can reach the rear side of the lowly doped Ge cell, whereas photons with shorter wavelengths are absorbed earlier in the layer stack. For the reflection, we distinguish between two regions. Region I between $E_{\Gamma 1}$ (1.55 $\mu$m) and $E_G$ (1.88 $\mu$m) where photons can be absorbed and contribute to $I_{\mathrm{SC}}$ and region II with wavelengths $>$1.88 $\mu$m corresponding to photons with energies which are too low to generate electron-hole-pairs in Ge. An enhanced reflection is beneficial for the cell performance in both regions: In region I, due to the increase in $I_{\mathrm{SC}}$ through carriers generated from photons absorbed during their second passage through the Ge cell after reflection and in region II due to enhanced out reflection and therefore a decrease in cell temperature under operation.

Indeed, the measured reflectivity of the three lowly doped isotypes with a mirror layer on the rear side (violet, red and blue in Fig. 5) is significantly higher than the measured reflectivity of the highly doped wafer with standard rear side (black) for all wavelengths longer than the wavelength of the direct Ge bandgap $E_{\Gamma 1}$ (1.55 $\mu$m). This difference in measured reflectivity increases for increasing wavelengths and reaches 40% for the standard cell, 81% for the AlOnly cell, 84% for the PassDop cell and the highest reflectivity of 85% for the LFC cell at 2.00 $\mu$m. The enhanced reflectivity in region I allows for a second passage of the photons through the Ge cell and enhance the absorption, attributing to the observed increase in $I_{\mathrm{SC}}$ in Figs. 3 and 4 together with the contribution of the passivation effect. The contribution of the mirror and the passivation effect on the increase in $I_{\mathrm{SC}}$ will be discussed further in the discussion section. The enhanced out-reflection up to 85% of photons in region II will decrease the cell temperature in operation. This decrease was published recently to be 9 °C in a similar cell type as investigated in this article [8].

## IV. Discussion

### A. Optimum Laser Pitch

As expected, a larger pitch (less contact points) leads to a larger unharmed passivation layer area on the Ge rear side. Therefore, $V_{\mathrm{OC}}$ increases slightly with the pitch for both LFC and PassDop isotypes. On the other hand, the series resistance $R_{\mathrm{S}}$ suffers from the larger distance between LFC points and therefore, FF decrease with increasing pitch. An idea to decrease $R_s$ without increasing the number of contact points is a laser power variation: An increase of the laser power causes an increase in diameter of the contact points. This could lead to a decrease in $R_S$ without destroying significantly more passivation layer. Therefore, the power variation between 2.1 and 7.0 W is performed for LFC samples with a pitch of 900 and 1000 $\mu$m (see appendix). The observed decrease in $V_{\mathrm{OC}}$ with increasing power shows a decrease of the passivation quality for larger contact points. This suggests that the introduction of additional defects and therefore additional recombination at the rear side and inside the Ge for increasing laser powers plays a more important role than a possible decrease in $R_S$ due to larger contacts. We conclude therefore that the optimized LFC process results from a laser power of 2.1 W and a pitch of 600 $\mu$m.

However, nearly the same cell results were obtained for pitches between 500 and 800 $\mu$m, which allows the statement that the LFC process is very robust toward laser parameter variation. For PassDop cells, no laser power variation was conducted due to the minor influence on cell performance observed for LFC samples. Analogously to the LFC cells, the PassDop cells processed with a laser power of 0.9 W and a pitch of 600 $\mu$m show the best cell results.

### *B. Improved Cell Performance*

The increase of all *I–V* parameters in the passivated isotypes in Figs. 3 and 4 compared to the AlOnly isotypes shows clearly that for lowly doped Ge, a rear side passivation and mirror layer improves the solar cell performance. The increase in $V_{\mathrm{OC}}$ is resulting from the passivation of the Ge rear side. The increase in $I_{\mathrm{SC}}$ is attributed to the lower doped Ge in combination with passivation and mirror layer on the rear side. The latter was proven experimentally by the EQE measurement in Fig. 5, were the EQE curves of the LFC and the PassDop samples are significantly higher than the EQE of the AlOnly cell in the wavelength range $>$1.55 $\mu$m ($<$0.80 eV), which correspond to the rear side of the cell.

We will now compare the experimental *I–V* parameters with the simulation results, which are indicated by a green horizontal line in Figs. 3 and 4. The values used for the simulations are given in Table I. For the standard cell, we observe a good agreement for $I_{\mathrm{SC}}$ and FF. However, $V_{\mathrm{OC}}$ and therefore the efficiency $\eta$ measured in the standard cell are lower ($\approx$12 mV and 0.2%$_{\mathrm{abs}}$) than in the simulation. However, larger standard cells show 10 mV higher $V_{\mathrm{OC}}$ which is very close to the simulated $V_{\mathrm{OC.}}$ Thus, we attribute this to process fluctuations in the manufacturing of the standard cells.

The measured improvements between the AlOnly cell and LFC/PassDop cells in $V_{\mathrm{OC}}$ due to rear side passivation and mirror for lowly doped Ge correspond very well to the simulated values ($\Delta V_{\mathrm{OC,sim}} \approx 52$ mV). The simulation of $V_{\mathrm{OC,sim}}$ allows for access to the passivation quality of the Ge rear side via the SRV. From our simulations, an SRV of 900 $\pm$ 180 cm/s was derived, which corresponds to a moderate passivation quality compared to lifetime samples, which reach SRV in the low tens cm/s range [10], [11]. This suggests that the solar cell process affects the Ge rear side passivation quality and that there is room for improvement, for example by protecting the unpassivated Ge rear side during the MOVPE process.

The measured trends in FF and $I_{\mathrm{SC}}$ are reproduced by the simulations. However, we expected a $I_{\mathrm{SC}}$ gain due to the passivation of $\Delta I_{\mathrm{SC,sim}} \approx 2$ mA.cm$^{-2}$ from the simulation which is higher compared to the measured gain ($\Delta I_{\mathrm{SC,meas}} \approx 1$ mA.cm$^{-2}$). This leads to an overestimation of the efficiency $\eta$ of $\approx$0.2% for the passivated cells.

Note that the $I_{SC}$ gain due to rear side passivation is less sensitive on the SRV compared to $V_{\mathrm{OC}}$ and the simulations provide the maximum performance for a given recombination velocity. The most probable reason for this deviation is the absorption dataset on which the simulation is based. It is difficult to distinguish between intrinsic and extrinsic (free carrier) absorption in doped Ge. We used a data set for doped Ge which leads to an overestimation of the intrinsic absorption, leading to an overestimation of $I_{\mathrm{SC}}$. It was beyond the scope of this article to solve this issue, but it will be subject of future work.

The FF gain for PassDop cells expected from the simulations overestimates slightly the experimentally found FF gain ($\Delta$FF = 5%$_{\mathrm{abs}}$ instead of $\approx$4%$_{\mathrm{abs}}$ in the measurements). The deviation in FF for LFC solar cells is significantly higher and is explainable with higher contact resistance for point contacts fabricated by the LFC concept. The increased contact resistance corresponds to an increase of the external series resistance in the simulation from 0.6 to 0.9 $\Omega$cm$^2$.

The measured improvements of the LFC and PassDop cells compared to the AlOnly cells proof successfully the passivation and mirror effect. However, for a real assessment of the rear side concept, the LFC and PassDop cells must be compared to standard cells from AZUR, which is also done in Figs. 3 and 4. The lowly doped Ge in our Ge-isotypes leads to an increase in current compared to the standard cell, even in the unpassivated AlOnly cell ($I_{\mathrm{SC,AlOnly}} \approx 28.0$ mA.cm$^{-2}$), but to a decrease in voltage, fill factor and efficiency ($V_{\mathrm{OC,AlOnly}} \approx 0.19$ V, $\mathrm{FF}_{\mathrm{AlOnly}}$ $\approx$ 0.57 and $\eta_{\mathrm{AlOnly}} \approx$ 2.26%). A lower $V_{\mathrm{OC}}$ for lower doping concentration $N_A$ is expected from theory, as the Fermi level splitting decreases with doping as shown

$$V_{\mathrm{OC}} = \frac{k_B T}{q} \ln\left(\frac{(N_A + \Delta n)\Delta n}{n_i^2}\right) \tag{1}$$

with the Boltzmann constant $k_B$, the temperature $T$, the elemental charge $q$, and the intrinsic/excess carrier concentration $n_{\mathrm{i}}/\Delta n$. For a good passivation, $V_{\mathrm{OC}}$ increases and becomes a function of the passivation quality, represented by the saturation current $I_0$ in

$$V_{\mathrm{OC}} = \frac{n k_B T}{q} \ln\left(\frac{I_{SC}}{I_o} - 1\right) \tag{2}$$

where $n$ is the ideality factor. We observe this increase in $V_{\mathrm{OC}}$ in our passivated isotypes, which reach the same $V_{\mathrm{OC}}$ ($\approx$0.25 V) as the standard isotypes—despite the lower doping. For $I_{\mathrm{SC,}}$ a maximum gain of 1.6 mA.cm$^{-2}$ between the standard isotypes and the passivated isotypes is reached.

We state that the presented cell concept leads to an experimentally shown increase in $I_{\mathrm{SC}}$ and to a $V_{\mathrm{OC}}$ comparable to standard cells. The gain in $I_{\mathrm{SC}}$ makes the concept interesting for new cell concepts with four or more junctions, which can benefit from higher Ge cell currents.

### *C. Influence of Mirror and Passivation on $I_{SC}$*

So far, we observed an increase in $I_{\mathrm{SC}}$ for all lowly doped isotypes (AlOnly, PassDop, and LFC) compared to the AZUR standard cell. Furthermore, the EQE and *%R* data confirms this gain in $I_{\mathrm{SC}}$ to arise from photons with energies lower than the direct bandgap $E_{\Gamma 1}$. However, to distinguish between the contribution of the lowly doped Ge in combination with the mirror and of the passivation effect on the increased $I_{\mathrm{SC}}$, a closer look at the experimental EQE and *%R* data is necessary. Therefore, the relative gain in relation to the AZUR standard isotype for EQE (straight lines) and *%R* (dotted lines) for all three lowly doped isotypes is presented in Fig. 6 in the wavelength range between the direct and the indirect band gap $E_{\Gamma 1}$ and $E_G$.

The strong modulation of *%R* and EQE especially in Fig. 6 results from the comparison with the AZUR standard sample,

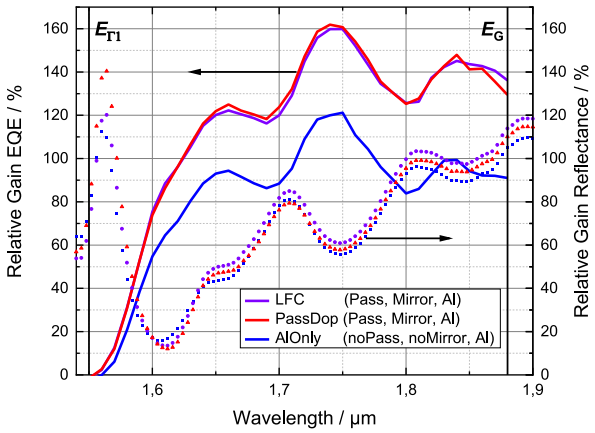


Fig. 6 Relative gain in $\%R$ and EQE against the standard Ge-isotype cell from AZUR for Ge-isotypes with passivation and mirror on rear side and a 600 $\mu$m pitch LFC contact (violet), a PassDop contact (red) and a Ge-isotype AlOnly cell without passivation but full-area Al contact on the Ge rear side (blue). The direct ($E_{\Gamma 1}$) and indirect ($E_G$) Ge bandgap correspond to the start and the end of the $x$-axes.

which shows strong thin film modulations (cf. Fig. 5, black line). These modulations require no further interpretation and will be ignored in the following considerations. A gain in reflection is observed in Fig. 6 compared to the standard cell for all three isotypes, showing clearly that the lowly doped Ge (less FCA) in combination with the Al rear side is the main reason for enhanced reflection. The fact that $\%R$ of the PassDop and the LFC sample at $E_G$ is enhanced compared to the AlOnly sample proves that the additional SiC passivation layer between Ge and Al increases the rear side reflection slightly for long wavelength.

Ignoring the modulation effect, the gain in EQE follows the increasing gain in %R from 1.6 $\mu$m until $E_G$. This proofs that the lower FCA due to lowly doped Ge in combination with the mirror effect contributes to the increase in $I_{SC}$. However, in the whole wavelength range, the relative gain in EQE of the passivated samples (violet/red) exceeds the relative gain of the AlOnly sample (blue) significantly, raising continuously from 20% difference at 1.6 $\mu$m to 50% difference near $E_G$. As there is no significant difference in reflection, we attribute this gain in EQE to the influence of the passivation effect. Both, the lowly doped Ge in combination with the Al reflector and the improved rear side passivation by $Si_xC_{1-x}$ contribute to the observed increase in $I_{SC}$ for lowly doped Ge-isotypes with improved rear side.

### D. Comparison Passdop and LFC Process

An improved back side technology was developed for Ge solar cells including a PassDop and LFC process route which both lead to an improved $I_{SC}$ and $V_{OC}$. This is due to the use of lowly doped Ge (lower FCA) in combination with an improved rear side passivation quality and a high reflection of photons if compared to a standard Ge cell with diffused contact. For both concepts, the cell parameters only vary slightly for a wide range of laser parameters.

The slightly lower $V_{OC}$ for PassDop isotypes compared to LFC isotypes suggests a more efficient $p^+$ doping for LFC isotypes by Aluminum compared to PassDop isotypes by the Boron in the passivation layer. On the other hand, the simulations showed a slightly higher $R_s$ for LFC isotypes compared to PassDop isotypes. From a practical point of view, the PassDop process is more promising for III-V applications, as it gets along with less energy input into the samples. The melting and solidification of Al in the LFC process leads to thermal expansion and subsequent shrinkage and therefore to strain in the rear side of the cell. Moreover, the LFC process is restricted to the use of Al as rear side metal; whereas for the PassDop cells, all highly reflective metals can be considered as rear side contact. Considering this variety of advantages of the PassDop process compared to the LFC process, we suggest to focus on the improvement of the former. The first step to enhance the passivation quality would be by improving the LBSF under the PassDop contacts. Therefore, a larger amount of boron or a change to gallium as dopant during deposition of the $Si_xC_{1-x}$ passivation layer seems to be the obvious next step.

## V. Conclusion

We aimed for a better low energy photon conversion in the Ge subcell for III-V multi junction solar cell devices. Therefore, the number of photons lost in the Ge bulk by FCA was reduced by using lowly doped Ge in combination with two rear side contact routes from Si photovoltaics. For both contact types, the rear side of the Ge cell consists of an a-$Si_xC_{1-x}$:H passivation layer stack followed by an Al layer. In both cases, the a-$Si_xC_{1-x}$:H passivation stack is opened with a laser process to generate point contacts, once before the Al deposition (PassDop concept) and once after the Al deposition (LFC concept). Both routes lead to Ge-isotypes with an increased $I_{SC}$ of up to 1.6 mA.cm$^{-2}$ and same $V_{OC}$ as standard Ge-isotypes, due to a successful rear side passivation by the a-$Si_xC_{1-x}$:H layer and high reflectivity due to the mirror effect of the a-$Si_xC_{1-x}$:H in combination with the Al layer. Corresponding solar cell simulations reveal a surface recombination velocity of 900 cm/s, which corresponds to a moderate passivation quality at the Ge rear side. This can be further improved in the future. Good PassDop and LFC cell results were obtained in a wide range of laser parameters with maximum efficiency for a laser pitch of 600 $\mu$m and a laser power of 2.1 W (LFC) and 0.9 W (PassDop). However, we recommend focussing on the further development of the PassDop concept, as the process is more gentle and flexible. These results suggest that the implementation of a passivated, highly reflecting rear side into III-V MJ solar cells should be considered for new cell concepts with enhanced current demand from the Ge subcell and for all III-V cell concepts which profit from a lower operation temperature due to enhanced out-reflection of subbandgap photons.

## Appendix

### A. Laser Power Variation

For LFC isotypes, not only a pitch, but also a laser power variation between 2.1 and 7.0 W was performed for two pitches (900 and 1000 $\mu$m). This corresponds to contact radii between 22 and 35 $\mu$m and areas covered with contacts between 0.2 and 0.5% (900 $\mu$m pitch) and 0.2 and 0.4% (1000 $\mu$m pitch).The $I$–$V$ results are shown in Fig. 7. $I_{SC}$ and FF increase slightly

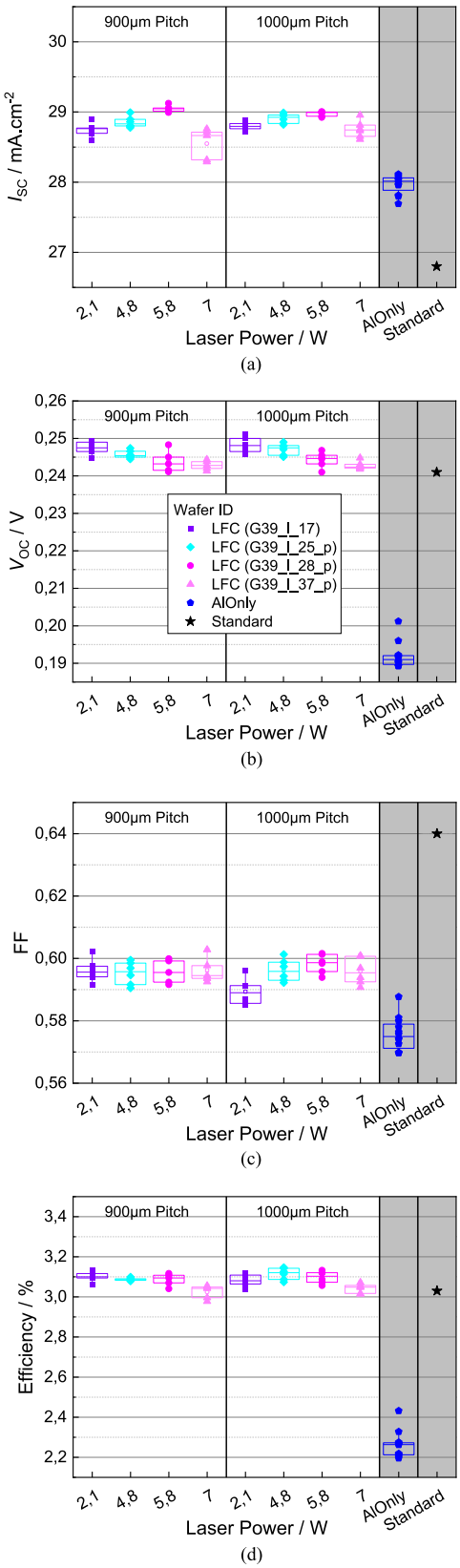


Fig. 7. *I–V* characteristics for Ge-isotypes with LFC rear side and with power variation for 900 and for 1000 $\mu$m. Data points with same colours and shapes belong to same wafers. On every wafer, there are 12 cells with two different pitches. Additionally, 12 AlOnly cells (blue pentagons) are measured and typical values for a standard cell (black stars) are depicted. (a) Parameter $I_{SC}$. (b) $V_{OC}$. (c) Fill factor. (d) Efficiency $\eta$.

with increasing power up to 5.8 W and drop at 7 W. This suggests an improved $R_S$ for powers up to 5.8 W. For 7 W, the high laser power starts to destroy the rear side and the cell parameters start to decrease. A continuous decrease in $V_{OC}$ with increasing power suggests a decrease of the passivation quality for larger contact points. The introduction of additional defects and therefore additional recombination at the rear side and inside the Ge is very likely. This leads to the best cell efficiency $> 3.1\%$ for a laser power of 4.8 W. However, the efficiency for cells treated with the initial laser power of 2.1 W and with pitches between 500 and 800 $\mu$m are still better [see Fig. 3(d)]. Due to this results, no power variation experiment was done for PassDop isotypes.

## REFERENCES


[1] J. F. Geisz *et al.*, "Building a six-junction inverted metamorphic concentrator solar cell," *IEEE J. Photovolt.*, vol. 8, no. 2, pp. 626–632, Mar. 2018.

[2] F. Dimroth *et al.*, "Four-junction wafer-bonded concentrator solar cells," *IEEE J. Photovolt.*, vol. 6, no. 1, pp. 343–349, Jan. 2016.

[3] R. M. France, F. Dimroth, T. J. Grassman, and R. R. King, "Metamorphic epitaxy for multijunction solar cells," *MRS Bull.,* vol. 41, no. 3, pp. 202–209, 2016.

[4] W. Guter *et al.*, "Space solar cells –3G30 and next generation radiation hard products," in *Proc. E3S Web Conf.*, 2017, p. 3005.

[5] J. Fernández, S. Janz, D. Suwito, E. Oliva, and F. Dimroth, "Advanced concepts for high-efficiency germanium photovoltaic cells," in *Proc. 33rd IEEE Photovolt. Specialist Conf., Proc.*, 2008, pp. 1–4.

[6] O. Höhn *et al.*, "Development of Germanium-based wafer-bonded four-junction solar cells," *IEEE J. Photovolt.*, vol. 9, no. 6, pp. 1625–1630, Nov. 2019.

[7] M. Nedeljkovic, R. Soref, and G. Z. Mashanovich, "Predictions of free-carrier electroabsorption and electrorefraction in germanium," *IEEE Photon. J,* vol. 7, no. 3, Jun. 2015, Art. no. 2600214.

[8] D. Alonso-Álvarez, C. Weiss, J. Fernandez, S. Janz, and N. Ekins-Daukes, "Assessing the operating temperature of multi-junction solar cells with novel rear side layer stack and local electrical contacts," *Sol. Energy Mater. Sol. Cells*, vol. 200, 2019, Art. no. 110025.

[9] C. Weiss *et al.*, "Potential analysis of a rear-side passivation for multi-junction space solar cells based on germanium substrates," in *Proc. 7th World Conf. Photovolt. Energy Convers., Proc.*, 2018, pp. 3392–3396.

[10] C. Weiss *et al.*, "Electron and proton irradiation effect on the minority carrier lifetime in SiC passivated p-doped ge wafers for space photovoltaics," *Sol. Energy Mater. Sol. Cells*, vol. 209, 2020, Art. no. 110430.

[11] S. Janz *et al.*, "Amorphous silicon carbide rear-side passivation and reflector layer stacks for multi-junction space solar cells based on germanium substrates," in *Proc. 44th IEEE Photovolt. Specialist Conf., Proc.*, 2017, pp. 83–87.

[12] E. Schneiderlöchner, R. Preu, R. Lüdemann, and S. W. Glunz, "Laser-fired rear contacts for crystalline silicon solar cells," *Prog. Photovolt. Res. Appl.*, vol. 10, no. 1, pp. 29–34, 2002.

[13] B. Steinhauser, U. Jäger, J. Benick, and M. Hermle, "PassDop rear side passivation based on $Al_2O_3$/a-$SiC_x$: B stacks for p-type PERL solar cells," *Sol. Energy Mater. Sol. Cells*, vol. 131, pp. 129–133, 2014.

[14] T. Rachow *et al.*, "Solar cells with epitaxial or gas phase diffused emitters above 21% efficiency," *Energy Procedia*, vol. 77, pp. 540–545, 2015.

[15] E. Simoen and C. Claeys, "Diffusion and solubility of dopants in germanium," in *Germanium-based Technologies: From materials to Devices*, 1st ed., C. L. Claeys and E. Simoen, Eds., Amsterdam, The Netherlands: Elsevier, 2007, pp. 67–96.

[16] A. Sanson *et al.*, "Investigation of germanium implanted with aluminum by multi-laser micro-Raman spectroscopy," *Thin Solid Films*, vol. 541, pp. 76–78, 2013.

[17] D. J. Friedman and J. M. Olson, "Analysis of ge junctions for gainp/gaas/Ge three-junction solar cells," *Prog. Photovolt. Res. Appl.*, vol. 9, no. 3, pp. 179–189, 2001.

[18] *SentaurusTM User Guide, Release I-2013.12,*Synopsys, Mountain View, CA, USA, 2013. [Online]. Available: https://www.synopsys.com/silicon/tcad/device-simulation/sentaurus-device.html

[19] V. Palankovski and R. Quay, *Analysis and Simulation of Heterostructure Devices*, 1st ed., S. Selberherr, Ed., Vienna, Austria: Springer, 2004.